Influence of steam-calcination and acid leaching treatment on the VGO hydrocracking performance of faujasite zeolite

Fuel Processing Technology 133 (2015) 89–96

Contents lists available at ScienceDirect

Fuel Processing Technology

journal homepage: www.elsevier.com/locate/fuproc

Influence of steam-calcination and acid leaching treatment on the VGO hydrocracking performance of faujasite zeolite

J.L. Agudelo [a], E.J.M. Hensen [b], S.A. Giraldo [a,*], L.J. Hoyos [c]

[a] Centro de Investigaciones en Catálisis (CICAT), Universidad Industrial de Santander, Cra. 27 Calle 9, Bucaramanga, Colombia
[b] Schuit Institute of Catalysis, Eindhoven University of Technology, P.O. Box 513, 5600 MB Eindhoven, The Netherlands
[c] Instituto Colombiano del Petróleo—ICP, ECOPETROL S.A., Km 7 vía a Piedecuesta, Piedecuesta, Colombia

ARTICLE INFO

Article history:
Received 12 October 2014
Received in revised form 7 January 2015
Accepted 11 January 2015
Available online xxxx

Keywords:
Hydrocracking
USY zeolite
Extraframework aluminum
Vacuum gas oil
Hydrothermal treatment
Acid leaching

ABSTRACT

The effect of hydrothermal treatment and mild acid leaching on the physico-chemical properties of zeolite Y and its vacuum gas oil hydrocracking performance was investigated. Ultra-stabilized Y (USY) zeolites were obtained by steam-calcination at 500, 600 and 700 °C. Steam-treated zeolites were further subjected to a mild acid leaching treatment. The zeolite samples were characterized by XRD, elemental analysis, XPS, N_2 adsorption, ^{29}Si and ^{27}Al NMR and FTIR spectroscopy of adsorbed pyridine. Steam-calcination resulted in dealumination and with increasing severity the micropore surface area and the framework Al content decreased. At the same time, the Al content at the zeolite crystal surface increased. Acid leaching improved the pore accessibility and acid properties due to the extraction of extraframework Al species (EFAl). NiMoP-based hydrocracking catalysts were prepared from the modified USY zeolites with alumina as binder. Hydrocracking activities correlated with the acidity of the zeolites. Too severe steam treatment led to depopulation of acid sites and lowered the hydrocracking performance. Hydrocracking catalysts based on the acid leached zeolites were more active than the ones based on the corresponding steam-treated zeolites. It is based on the removal of agglomerated extraframework Al species that block the access to some of the micro- and mesopores. This study points out that, aside from the acidity, also other parameters such as pore accessibility and the presence of EFAl have considerable influence on the hydrocracking of the heavy molecules in a gas oil feed.

1. Introduction

Hydrocracking is one of the principal refinery processes due to its versatility to produce high-quality transportation fuels from a broad range of low-value heavy oil fractions [1,2]. In this technology the catalyst plays a key role in determining the product distribution [3]. Hydrocracking reactions are catalyzed by acid and metal functions. Metallic sites catalyze alkane/alkene (de)hydrogenation reactions, while the acid sites on the support crack alkenes to smaller product molecules. Amorphous silica-alumina (ASA) and ultra-stabilized Y (USY) zeolite are commonly used as acidic support in hydrocracking catalysts. Compared to ASA, USY zeolites contain a larger number of Brønsted acid sites, which are also of higher strength. A drawback of the use of zeolites is that their pores impose diffusion limitations during heavy feedstock processing [4]. In general, USY zeolite based hydrocracking catalysts yield less middle distillates than ASA-based ones. Historically, extensive research to relate textural and acidic properties of USY zeolite to its catalytic behavior has been done in the context of the Fluid Catalytic Cracking (FCC) process, which is primarily used to produce gasoline. It has led to detailed insight into the physico-chemical and catalytic properties of USY zeolites [5]. There are relatively few systematic studies about such structure–performance relations concerning hydrocracking of real feedstocks with the purpose of producing middle distillates [6,7]. Recent research has focused on the development of improved USY-based catalysts with high activity towards middle distillates [8–13], driven by the increased diesel demand in many countries [14].

Hydrocracking uses framework-dealuminated USY zeolites. Zeolite Y is dealuminated to limit its hydrogen transfer activity. In this way, the propensity to coke deactivation is diminished. In addition, dealumination is needed to convert the initially weak acid Y zeolite with a low framework Si/Al ratio into highly acidic ultra-stabilized Y zeolite. The selectivity in hydrocracking is mainly determined by the Brønsted acidity of the support, which closely correlates to the framework Si to Al ratio. For Y zeolite, the higher the degree of framework dealumination, the higher the middle distillates selectivity [15]. Highly dealuminated Y zeolites have comparable acidity to amorphous silica-alumina supports and, accordingly, offer similar high middle distillates selectivity. The low acidity of such materials results in low reaction rates, which needs to be compensated by higher

* Corresponding author. Tel.: +57 7 6344746; fax: +57 7 6344684.
E-mail addresses: sgiraldo@uis.edu.co, giraldosonia@yahoo.fr (S.A. Giraldo).

http://dx.doi.org/10.1016/j.fuproc.2015.01.011
0378-3820/

reaction temperature. Tuning the acidity of Y zeolite, therefore, remains a major topic in the design of active hydrocracking catalysts for middle distillates production. The approach is to use moderately dealuminated zeolites and optimize their acid and textural properties to obtain satisfactory conversion levels and middle distillates yield [16].

Typically, USY zeolites are prepared by combining hydrothermal treatment of Y zeolite and chemical modification methods [17]. The removal of framework Al atoms by hydrothermal treatment generates extraframework aluminum species (EFAl). The amount and nature of the EFAl species formed depend on the severity of the hydrothermal treatment step [18]. The presence of large amounts of EFAl has a negative effect on the catalytic and transport properties. On the other hand, it is known that some EFAl species are important to enhance the intrinsic acidity in USY zeolites [19]. The improved cracking activity of USY zeolites is believed to be influenced by synergistic interactions between framework and cationic EFAl species [20], and this topic has been subject of active debate in literature [21–23]. Hydrothermal treatment also results in loss of crystallinity and the development of a secondary pore system, reducing mass transport limitations and offering the possibility to convert a larger fraction of the feedstock. Chemical modification methods, in turn, are designed to improve zeolite properties such as mesoporosity and acid strength and density. Many modifying agents have been employed for this purpose such as mineral acids, organic acids, $(NH_4)_2SiF_6$, NaOH and EDTA [24]. Some of these methods have been employed with success to obtain suitable zeolites as the acidic component in hydrocracking catalysts [8,12,25,26].

The main goal of the present study was to determine the influence of the dealumination degree of USY zeolite on its hydrocracking performance. A significant body of knowledge exists in the field of modifying Y zeolite. However, there are relatively few studies that determine the influence of changes to the Y zeolite structure and acidity on the hydrocracking performance of a heavy feed in a systematic manner. Mild acid leaching was used to remove some of the deleterious EFAl species. The physico-chemical properties of the zeolites were determined by means of XRD, elemental analysis, XPS, N_2 adsorption, solid-state NMR (^{29}Si, ^{27}Al), and FTIR of adsorbed pyridine. Hydrocracking catalysts were prepared from the modified USY zeolites by loading a P-promoted NiMo-sulfide phase. Their performance was evaluated in the hydrocracking of a heavy vacuum gas oil. Although acidity is one of the main catalyst parameters, the results show that small variations in other properties will strongly affect the performance in the conversion of heavy feedstock molecules present in a VGO feed.

2. Experimental

2.1. Catalysts preparation

NH_4-Y zeolite with sodium content less than 0.15 wt% was obtained by threefold ion exchange of a commercial faujasite zeolite (CBV400, *Zeolyst International*). USY-HT500, USY-HT600 and USY-HT700 were obtained by hydrothermal treatment of portions of this NH_4-Y zeolite under 100% steam flow for 5 h at 500, 600 or 700 °C. Mild acid leaching was done by stirring the suspended HT zeolite in a 0.25 N HCl solution at 60 °C for 2 h. The resulting samples are denoted by the suffix AL (acid leaching). Composite hydrocracking catalysts were prepared from these hydrothermally treated and acid leached zeolites. The modified zeolite (40 wt%) was kneaded with alumina binder (Catapal B, *Sasol North America Inc.*) using a 1 wt% HNO_3 solution as peptizing agent. The resulting doughs were extruded into cylindrical shapes with a diameter of 1 mm. These catalyst bodies were dried, crushed and calcined at 550 °C for 6 h under static conditions. Subsequently, NiMoP-containing catalysts were prepared by sequential introduction via incipient wetness impregnation of P, Mo and Ni in the form of phosphoric acid (85 wt%, Merck), ammonium heptamolybdate tetrahydrate (99 wt%, Merck) and nickel nitrate hexahydrate (99 wt%, Merck). Intermediate drying at 105 °C for 15 h and calcination in oven at 500 °C for 2 h were performed after each impregnation step. The intended loadings were 1 wt% of P, 15 wt% of MoO_3 and 3 wt% of NiO.

2.2. Characterization

Nitrogen physisorption measurements were performed at 77 K on a Micromeritics ASAP 2020 instrument. The Brunauer–Emmett–Teller (BET) adsorption isotherm model was used to determine the total surface area. The pore size distributions (PSD) in the mesopore range were obtained from the adsorption branch of the isotherms with the Barrett–Joyner–Halenda (BJH) method.

The bulk chemical composition was determined by ICP-OES after proper digestion of the complete sample in a mixture of HF/HNO_3. XRD patterns were recorded on a Bruker D4 Endeavor diffractometer using CuKα radiation in the range of $5° \leq 2\theta \leq 60°$ with a step size of 0.0028° and a time step of 1 s. The unit cell size of the zeolites was determined by using a full pattern matching procedure with the TOPAS software.

High resolution transmission electron microscopy (HRTEM) images of the zeolite particles were taken on a FEI Tecnai 20 at an electron acceleration voltage of 200 kV. Prior to measurements the zeolite samples were suspended in ethanol, sonicated for 1 min, and dispersed over a carbon coated holey Cu grid.

IR spectroscopy of adsorbed pyridine was used to probe Brønsted and Lewis acidity. Spectra were recorded with a Bruker Vertex V70v instrument equipped with a home-made controlled-environment transmission cell and CaF_2 windows. Typically, a small amount of zeolite powder was pressed into a self-supported wafer. The wafer was heated for 1 h under vacuum to 550 °C at a rate of 10 °C/min. After cooling to 150 °C, a reference spectrum was taken. The sample was then exposed to pyridine until it was saturated. Physisorbed pyridine was removed by evacuation for 1 h at 150 °C. The resulting IR spectrum was used to determine the total acidity. Then, the sample was evacuated at 350 °C and 500 °C for 1 h and spectra were recorded at 150 °C after each desorption step. We used these spectra to determine the medium and strong acid sites. The densities of Brønsted (peak at 1550 cm^{-1}) and Lewis (peak at 1450 cm^{-1}) acid sites were determined by using the values for the molar extinction coefficients of 0.73 cm/mol 1.11 cm/mol, respectively [27].

Magic Angle Spinning (MAS) Nuclear Magnetic Resonance (NMR) spectra were recorded on a Bruker AVANCE III D400 NMR spectrometer operating at a magnetic field of 9.4 T. For the ^{27}Al MAS NMR a standard Bruker MAS probe head was used with 2.5 mm rotors spinning at a rate of 15 kHz. The ^{27}Al chemical shift was referred to a saturated $Al(NO_3)_3$ solution. ^{29}Si MAS NMR spectra were recorded using single pulse excitation (π/2 pulses) at a rate of 14 kHz. The ^{29}Si spectra were externally referenced to Q_8M_8 at 0 ppm. Quantitative line shape analysis of the ^{29}Si MAS NMR spectra was performed by using the Dmfit2011 software. Gaussian line shapes were used to deconvolute the NMR spectra.

UV–Vis diffuse reflectance spectroscopy (DRS) and Laser Raman spectroscopy (LRS) measurements were performed to the composite NiMoP hydrocracking catalysts in their oxide state. UV–Vis DRS spectra were recorded on a Shimadzu UV-2401 PC spectrometer in diffuse-reflectance mode with a 60 mm integrating sphere in the 200–800 nm range. BaSO4 was used as the reference. The spectra were transformed using the Kubelka–Munk function. Laser Raman spectra were recorded with a Jobin–Yvon T64000 triple stage spectrograph with spectral resolution of 2 cm^{-1} operating in double subtractive mode. The laser line at 325 nm of a Kimmon He–Cd laser was used as exciting source. The power of the laser on the sample was 4 mW.

Surface analysis by XPS spectroscopy was applied to characterize the sulfidability of the hydrocracking catalysts. Sulfidation of the samples

was done by heating typically 0.25 g of 50/80 mesh of the calcined NiMoP catalyst pellets in a stainless steel micro reactor in a mixed H_2S/H_2 flow (15 mol% H_2S) at a rate of 6 °C/min up to 400 °C; the final temperature was maintained for 2 h. The sample was then cooled to room temperature and the gas was switched to He. By closing valves before and after the reactor, the sample was transferred to a glove box under nitrogen atmosphere with controlled oxygen and water levels (both < 1 ppm) in order to avoid re-oxidation of the catalyst. The samples were crushed in a mortar and pressed onto a double-sided carbon tape attached to a sample holder. The sample holder was then transferred from the globe box to the introduction chamber of the XPS spectrometer under exclusion of air. XPS spectra were recorded on a KRATOS AXIS ULTRA instrument with an Al monochromator source (1486.6 eV) and a hemi-spherical analyzer operating at fixed pass energy of 40 eV and working under high vacuum ($<10^{-9}$ Pa). The Al 2p peak from the support at 74.5 eV was used as internal standard for binding energy calibration. The Mo 3d, Ni 2p, S 2p, Al 2p, O 1 s, and Si 2p spectra were analyzed using the software CasaXPS. A Shirley background subtraction was applied and a 30/70 Gaussian/Lorentzian ratio for peak decomposition was used.

2.3. Hydrocracking activity evaluation

Hydrocracking activity tests were performed with the NiMoP-based catalysts. The feedstock was a pre-treated vacuum gas oil with the following properties: density = 0.91 g/cm^3, S content = 43 ppm, N content = 25 ppm, and aniline point = 79.9 °C. The catalysts were placed in a stainless-steel tubular reaction system (*Parr Instruments*). In a typical run, 4.2 g of the catalysts was diluted with inert sand. The bed volume was approximately 8 cm^3. The catalysts were sulfided *in situ* following a slow heating ramp (10 °C/h) to 345 °C with a diesel feed containing 4 wt% of dimethyl disulfide and 0.5 wt% of aniline. The sulfidation temperature was maintained for 12 h before the VGO admission. The hydrocracking reaction conditions were 345 °C, 1500 psig, H_2/feed ratio 1250 NL/L, and the WHSV was 1 h^{-1}. Conversion was referred to the 370 °C$^+$ cut in the feed. Products were analyzed by simulated distillation by gas chromatography (SimDis-GC) according to the ASTM D7213 standard test method. Selectivity to middle distillates was referred to the fraction 180–370 °C in the product mixture. Selectivity to naphtha was referred to the fraction IPB–180 °C cut. Conversions values are reported from the average of several liquid product samples taken from 50 to 80 h on stream. The experimental error was determined to be below 2%. No deactivation was observed for the reaction times used to determine conversion. The gas product yields were less than 5% in all cases.

3. Results and discussion

3.1. Physicochemical properties of the zeolites

The most important properties including the surface areas and pore volumes, the unit cell parameters, the bulk, framework and surface Si/Al ratios of the modified zeolites are presented in Table 1. It is seen that the total surface area and micropore volume decrease with increasing temperature of the hydrothermal treatment step. At the same time, the mesopore and total pore volumes increase slightly. These changes are due to the structural collapse of the zeolite [3]. During hydrothermal treatment, Al atoms are extracted from the framework. Framework dealumination involves the disassembly of the sodalite cages and also some supercages, resulting in formation of mesopores with sizes in the range of 5–50 nm [19].

After HCl leaching, the micro- and mesoporosity of the zeolites hydrothermally treated at 500 and 600 °C (samples USY-HT500AL and USY-HT600AL) improved. The increase in the mesopore volume is in line with findings reported in literature [28]. It has been ascribed to the removal of EFAl species formed during steaming that block the pore system [29]. Acid leaching sample USY-HT700 results in a different behavior with little change in the textural properties. This is presumably because the chosen leaching conditions were too mild to extract the EFAl species present in the starting zeolite (USY-HT700).

Hydrothermal treatment did not change the bulk Si/Al ratios of the samples. On the contrary, acid leaching increased the bulk Si/Al as a result of the removal of Al. The degree of Al removal is, however, relatively low for the acid leaching treatment employed here. It is largest for the acid leached sample that was steam-treated at 500 °C. It has been established that the temperature of steam dealumination influences the EFAl speciation [30]. At higher steaming temperature the amount of polymerized EFAl species increases. The difficulty in removing EFAl species can therefore be related to their higher degree of agglomeration [18].

Framework Si/Al ratios gradually increase with the temperature of steaming (Table 1). This is expected and points to progressive dealumination of the framework [31]. There is also a significant difference between the bulk and framework Si/Al values for the hydrothermally treated samples. The difference becomes larger with the steaming temperature. This shows that more severe steam treatment results in more EFAl species. Comparison of the framework Si/Al ratios and the unit cell sizes before and after acid leaching shows that this treatment caused further dealumination of the framework. Accordingly, we conclude that acid leaching by HCl does not only remove EFAl species but also further dealuminates the framework.

Table 1
Textural properties and structural composition of the modified zeolites.

Property	USY-HT500	USY-HT600	USY-HT700	USY-HT500AL	USY-HT600AL	USY-HT700AL
S_{BET} (m^2/g)[a]	666	653	635	737	710	630
S_{micro} (m^2/g)[b]	599	575	551	650	620	549
V_{total} (cm^3/g)[c]	0.36	0.38	0.40	0.41	0.43	0.40
V_{micro} (cm^3/g)[d]	0.25	0.24	0.23	0.27	0.26	0.23
V_{meso} (cm^3/g)[e]	0.11	0.14	0.17	0.14	0.17	0.17
$(Si/Al)_{bulk}$	3.1	3.1	3.1	3.8	3.6	3.5
$(Si/Al)_{surface}$[f]	1.8	1.5	1.2	3.0	2.6	2.0
$(Si/Al)_{framework}$[g]	5.7	6.8	11.1	7.9	8.5	12.6
a_o (Å)[h]	24.389	24.359	24.334	24.396	24.346	24.300

[a] BET surface area.
[b] Microporous surface area.
[c] Total pore volume.
[d] Microporous pore volume (t-plot method).
[e] Mesoporous pore volume.
[f] From XPS.
[g] Framework Si/Al ratio from ^{29}Si MAS NMR.
[h] Unit cell size from XRD.

XPS analysis in Table 1 shows that surface Si/Al ratios are lower than the corresponding bulk values for the hydrothermally treated zeolites. It points to migration of EFAl species to the external surface of the zeolite crystals [32]. The migration of EFAl species is more substantial for the samples steamed at higher temperatures. For acid leached zeolites, the surface Si/Al increases, which implies removal of Al from the external surface region of the zeolite crystals. Al is assumed to be removed by dissolution of EFAl species and part of the remaining framework Al [33].

XRD diffraction patterns of the zeolites samples are included in Fig. S1 of the supporting information. The treatments do not drastically affect the crystalline order of the USY zeolites. Additionally, diffuse scattering effects from X-ray amorphous non-framework species such as silica and silica-alumina, which are typically observed in the 2θ region between 20° and 30°, remain low for all of the zeolite samples.

In brief, the results presented above show that an increasing amount of Al is removed from the framework with increasing hydrothermal treatment temperature. This treatment gradually lowers the micropore surface area by formation of mesopores. At the same time, the surface Si/Al decreases due to migration of Al to the external surface region of the zeolite crystals. Acid leaching extracts some of the EFAl species and, consequently, improves the accessibility of the micropores and mesopores. Acid leaching also leads to some further framework dealumination.

The pore size distributions (PSD) in the mesopore range are given in Fig. S2 of the supporting information. All materials have a relatively wide distribution of mesopore sizes with maxima at 160 Å for USY-HT500 and USY-HT600; upon acid treatment, the maxima shift to 220 Å, which should be the consequence of the removal of polymerized EFAl that obstruct the mesopore system. USY-HT700 and USY-HT700AL zeolites have similar mesopore size distributions. The observed trends are in line with the changes in textural properties presented in Table 1.

The morphology of the zeolite particles and the mesopore network were examined by high resolution transmission electron microscopy (HRTEM). Fig. 1 presents representative HRTEM images of the USY-HT600 and USY-HT600AL zeolites. The images indicate that the morphology of the grains, as shown in Figs. 1a and b, is not uniform in neither the steam-treated nor the acid-leached zeolite. Additionally, by comparison of several images before and after acid leaching (not shown), it is deduced that the acid treatment did not result in fragmentation of crystals; accordingly, considerable changes in the overall zeolite morphology due to the acid treatment are absent. Fig. 1b also reveals the characteristics of the mesopore system in the acid-treated zeolite. Mesopores are distinguishable as lighter zones, typically concentrated in the interior of the grains, while the smooth dark zones relate to the unaffected microporous regions of the crystals. In this zeolite sample, some intra-crystalline voids coalesce to form channel-like mesopores. In general, an inhomogeneous distribution of mesopores is observed among different zeolite grains and within individual grains. Fig. 1c presents an image of a USY-HT600 zeolite crystal at increased magnification. Some crater-like mesopores at the exterior surface of the zeolite particle are clearly noticeable. These mesopores have pore diameters close to the average value obtained from the nitrogen adsorption data (Fig. S1 in supporting information).

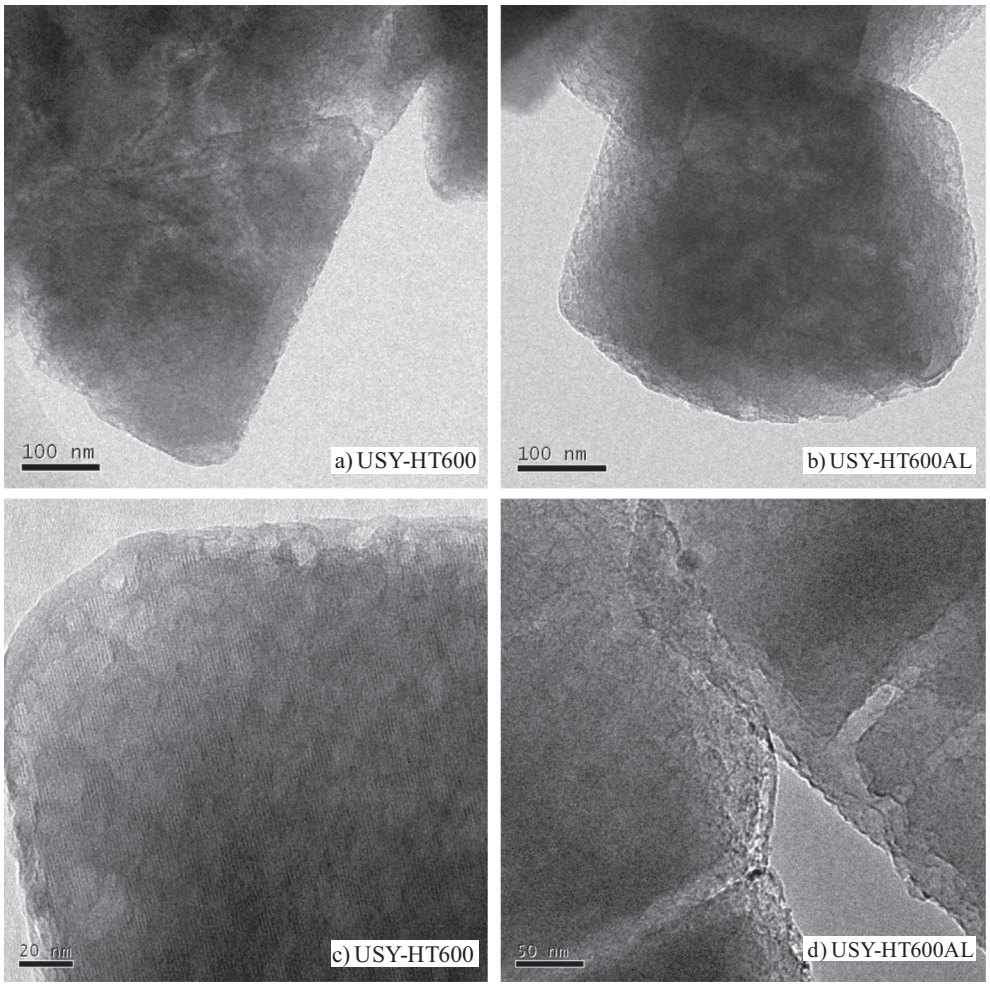

Fig. 1. HRTEM images of USY-HT600 and USY-HT600AL zeolites.

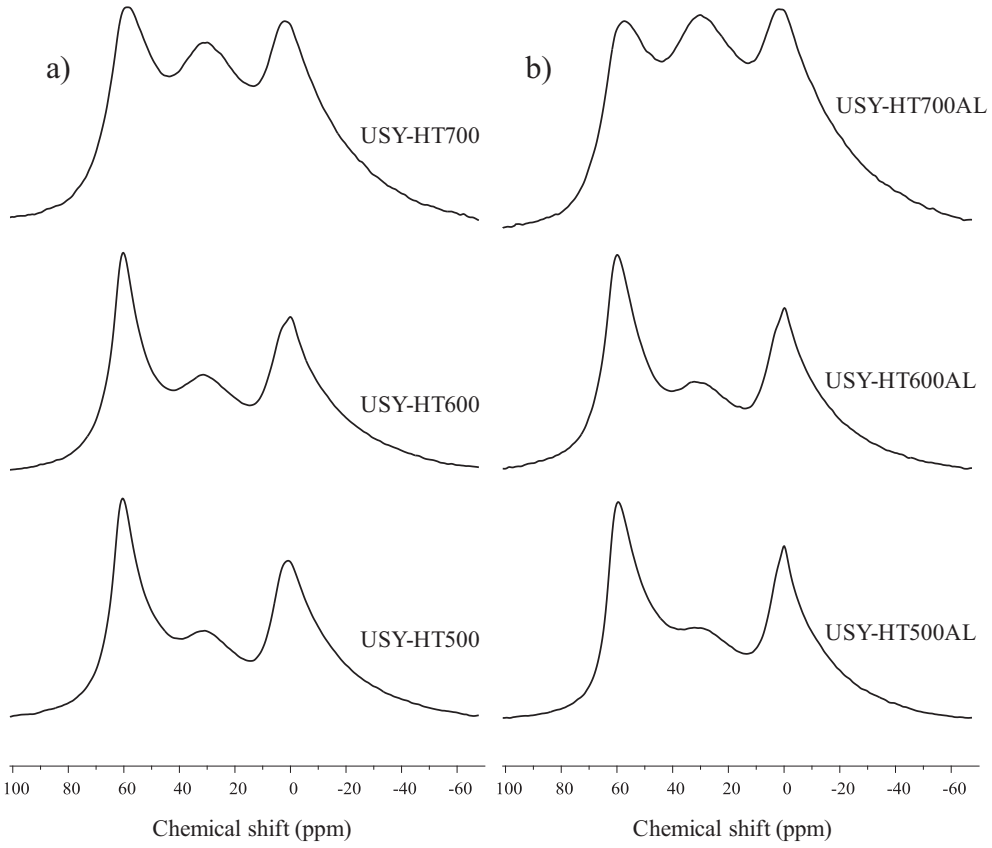

Fig. 2. ^{27}Al MAS NMR spectra of the hydrothermally and acid treated zeolites. (a) Steam-treated zeolites and (b) acid-leached zeolites.

Fig. 1d shows the formation of channels along crystals defects in the USY-HT600AL zeolite, visibly connected to the outer surface of the crystals. The features observed by HRTEM are in general agreement with other studies of chemically-treated USY zeolites [8,19].

3.2. ^{27}Al MAS NMR characterization

The evolution of the coordination of the Al species in the samples due to hydrothermal and acid leaching treatments was followed by ^{27}Al NMR spectroscopy. Three main peaks are observed in the spectra for all of the zeolites shown in Fig. 2, namely at 60, 30 and 0 ppm. The signals at 60 and 0 ppm are due to Al nuclei in tetrahedral and octahedral coordination environment, respectively [33–35]. The signal at 30 ppm is assigned to distorted tetrahedral or five-coordinated Al species [35–37]. Increasing the temperature of hydrothermal treatment from 500 to 600 °C increases the 30 ppm band (Fig. 2a). For the sample steam-treated at 700 °C the contributions of the three main bands becomes nearly equal, which points to the highest degree of dealumination and considerable heterogeneity in the Al coordination. Acid leaching causes the decrease of the band at 30 ppm and sharpening of the octahedral Al region in samples USY-HT500AL and USY-HT600AL (Fig. 2b). It points to removal of EFAl species. Nevertheless, a significant amount of EFAl species (penta- and hexa-coordinated Al) resisted acid leaching. According to literature, acid leaching removes preferentially amorphous material and Al linked to the framework [37,38]. The changes in the NMR spectra therefore indicate that a separate extraframework silica-alumina phase is removed by acid leaching. The EFAl contribution is highest in the USY-HT700AL sample with respect to its parent zeolite USY-HT700. This result indicates that the acid leaching of the USY-HT700 sample was not as effective as for the milder steamed samples, presumably because of the higher degree of agglomeration of the EFAl phase. The ^{27}Al MAS NMR data agree with the structural characterization results presented in Table 1 with respect to the framework Al content and the degree of bulk dealumination following acid leaching treatment.

3.3. Acid properties characterization

3.3.1. FTIR spectroscopy of hydroxyl groups

The Brønsted acidity of zeolites is mainly related to bridging hydroxyl groups. Infrared spectra of the zeolite samples in the OH stretching region are presented in Fig. 3. The spectra show at least five bands at around 3562, 3600, 3625, 3670 and 3739 cm^{-1}. However, all of these bands are overlapped by other OH stretching vibrations [39]. The bands at 3562 and 3625 cm^{-1} correspond to bridged Si-(OH)-Al Brønsted acid sites located in the sodalite cages (low-frequency, LF) and in the supercages (high-frequency, HF), respectively [40]. The band at around 3600 cm^{-1} is attributed to a high-frequency OH group, perturbed by the interaction with Lewis sites present in EFAl species generated during steam dealumination [41]. The band at 3670 cm^{-1} is assigned to hydroxyl groups of Al-OH species present in extraframework positions [42]. The asymmetric band with maximum at 3739 cm^{-1} corresponds to the superposition of several types of silanol groups [43].

According to Fig. 3, when the temperature of hydrothermal treatment increases from 500 to 600 °C (spectra a and c), the amount of HF and LF hydroxyl groups slightly diminished. However, steam treatment at 700 °C (spectrum e) led to a strong decrease of the intensities of the HF and LF OH bands. It shows considerable framework dealumination and lowering of the Brønsted acidity. At the same time, structural defects developed, as indicated by the sharpening of the signal at 3739 cm^{-1} assigned to terminal Si–OH groups. Acid leaching mainly affects the intensity of the band at 3600 cm^{-1} for the zeolite hydrothermally treated at 500 °C (spectra a and b). For the other two steam-treated zeolites, the effect of acid leaching is very small. The band at

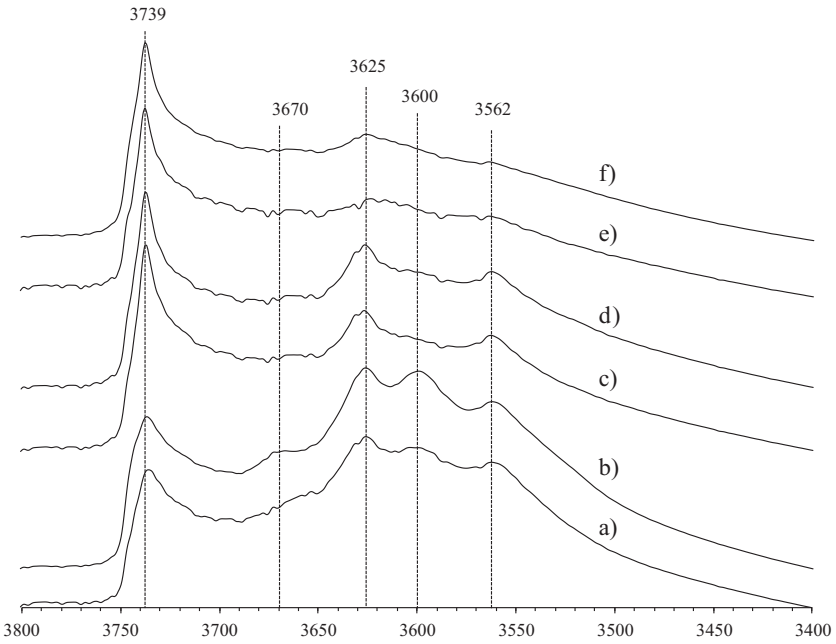

Fig. 3. FTIR spectra in the OH region for the zeolite samples. (a) USY-HT500, (b) USY-HT500AL, (c) USY-HT600, (d) USY-HT600AL, (e) USY-HT700, and (f) USY-HT700AL. Positions for the main bands are indicated with dashed lines. Spectra were taken at 150 °C after evacuation in vacuum at 500 °C.

around 3600 cm^{-1} has been extensively discussed in literature, because it has been linked to the increased acidity usually observed in USY zeolites [23,44].

3.3.2. FTIR measurements of adsorbed pyridine

Further acidity characterization was done by FTIR spectroscopy of adsorbed pyridine. The data are reported in Table 2. It is seen that higher hydrothermal treatment temperature led to zeolites with lower Brønsted acid site content. This can be directly correlated to framework dealumination. At the same time, the fraction of strong Brønsted acid sites is also decreasing (B_{strong}/B_{total} ratios). Acid leaching increases the total number of Brønsted acid sites, mainly by increasing the number of medium and strong acid sites for zeolites hydrothermally treated at 500 and 600 °C. The zeolite steam-treated at 700 °C and its acid-leached counterpart (USY-HT700AL) behave differently. The increase in Brønsted acid site content after acid leaching can be explained by enhanced access of pyridine to the inner parts of the zeolite, because polymerized Al species obstructing the pore system have been partially removed. The increase in acid strength shown by the acid leached zeolites USY-HT500AL and USY-HT600AL is explained by the removal of some non-framework aluminum species acting as charge-balancing cations [29]. The pyridine FTIR results also show that the Lewis acid site content was slightly decreased by the acid leaching treatment in all cases. This can be directly related to the removal of EFAl species. Acid leaching of USY-HT700 results in a zeolite with a higher Lewis to Brønsted acid site ratio (USY-HT700AL) than the other samples.

In summary, acidity characterization shows that increasing severity of the steam-calcination step lowers the amount of Brønsted acid sites. This is a consequence of framework dealumination. Acid leaching treatment significantly increases the number of medium and strong Brønsted acid sites, presumably as a result of the removal of charge-balancing EFAl species. Removal of these and more agglomerated forms of EFAl leads to better accessibility of the acid sites.

3.4. Hydrocracking activity of NiMoP-supported catalysts

Hydrocracking catalysts were prepared by loading the NiMoP components on the supports based on the modified zeolites and alumina. The resulting catalysts were sulfided and evaluated for their performance in the hydrocracking of a heavy VGO feedstock. As exemplified in literature [8,10,12,45,46], differences in catalytic activity in VGO hydrocracking can be related to the zeolite component as long as the other properties such as the hydrogenation function and catalyst loading are kept the same. To support this supposition, the final hydrocracking catalysts were characterized by nitrogen physisorption, UV–Vis DRS, Laser Raman spectroscopy (LRS) in calcined form and XPS surface

Table 2
Acidity characterization by FTIR spectroscopy of adsorbed pyridine.

Zeolite	Brønsted acid sites (mmol/g)			Lewis acid sites (mmol/g)			B_{strong}/B_{total}[d]	L_{total}/B_{total}[e]
	Total[a]	Medium[b]	Strong[c]	Total	Medium	Strong		
USY-HT500	0.56	0.44	0.13	0.61	0.44	0.35	0.23	1.09
USY-HT500AL	0.66	0.54	0.20	0.57	0.39	0.33	0.30	0.86
USY-HT600	0.40	0.28	0.07	0.45	0.33	0.26	0.18	1.13
USY-HT600AL	0.43	0.31	0.08	0.41	0.27	0.22	0.19	0.95
USY-HT700	0.29	0.18	0.03	0.32	0.21	0.15	0.10	1.10
USY-HT700AL	0.22	0.15	0.03	0.28	0.19	0.15	0.14	1.27

[a] Acid sites after desorption at 150 °C.
[b] Acid sites after desorption at 300 °C.
[c] Acid sites after desorption at 500 °C.
[d] Strong Brønsted acid sites over total Brønsted acid sites.
[e] Total Lewis acid sites over total Brønsted acid sites.

analysis after sulfidation in H_2S/H_2 flow. The nitrogen physisorption results indicate that the textural properties of the hydrocracking catalysts follow the trends seen for the parent zeolites (not shown). The further characterization of the NiMoP-supported catalysts showed only minor differences in the dispersion of the NiMo-oxide components and in the metal-support interactions. In brief, UV–Vis DRS results indicate that the different characteristics of the modified zeolites in the supports do not influence the coordination of the supported Mo and Ni (Fig. S3 in supporting information). According to LRS results (Fig. S4 in supporting information), the lack of two sharp and intense peaks at 995 and 820 cm^{-1} characteristic of free MoO_3 aggregates points out that Mo is well dispersed on the carrier materials. XPS analysis indicates that all the catalysts can reach similar sulfidation degrees and NiMoS phase contents independently of the features of the zeolite component in the support (Tables S1 and S2 of supporting information). The above observed behaviors are to be expected because the (de)-hydrogenation components will be mainly deposited on the alumina part of the composite catalysts because the incorporation of Mo into the porous structure of the zeolite is usually restricted [47,48].

Hydrocracking activities and the ratio of the middle distillate to naphtha yields are presented in Table 3. For hydrocracking catalysts based on the non-acid-leached zeolites, the conversion of the 370 °C^+ VGO fraction decreased with increasing steaming temperature. The catalysts based on USY-HT500AL and USY-HT600AL display significantly higher VGO hydrocracking activities compared with catalysts based on the corresponding steam-treated zeolites. The catalyst based on the USY-HT700AL zeolite shows different behavior in the sense that the activity decreased upon acid leaching. The ratio of the middle distillates and naphtha yields follows expectedly the reverse trend, namely that it increases with decreasing conversion. All of the above observations in the VGO hydrocracking performance can be directly related to changes in the textural and/or acid properties of the zeolite component of the hydrocracking catalysts (Tables 1 and 2). These trends will be discussed briefly below.

Overall, the steam treatment of the parent zeolite led to structural collapse of the zeolite due the extraction of framework Al species. It resulted in a decrease of the total and micropore surface area, the unit cell size and, most importantly, the Brønsted acidity. The degree of dealumination increased with increasing steam-treatment temperature. As a result of the lower acidity, the VGO hydrocracking conversion decreased for zeolites treated at more severe conditions. Upon acid leaching, catalysts made from USY-HT500AL and USY-HT600AL showed improved hydrocracking activity as compared to catalyst prepared from their steam-treated parents. It is the consequence of increased accessibility due to EFAl removal. The improved conversion of the heavy end of the VGO feed is due to the increased mesopore surface area of the zeolites upon acid leaching. It may be safely assumed that hydrocracking of VGO over USY zeolites is a diffusion-controlled reaction, because the bulky compounds in the feed with up to 40 carbon atoms per molecule cannot enter the micropores. Only a small portion of acid sites can interact with these heavy oil molecules [49]. Therefore, the development of an additional mesopore system during steaming and improvement of its accessibility due to acid leaching by removal of polymerized EFAl species from the mesopores and the pore mouths facilitates the transport of heavy molecules from the bulk to the active sites [8]. The leaching of EFAl species was evident from the combination of chemical analysis, XRD, XPS, and ^{27}Al MAS NMR spectroscopy. The second effect of acid leaching is that the density of Brønsted acid sites increased. This is most likely due to the removal of EFAl species, opening up the pore structure as well as the removal of charge-balancing EFAl cations.

In the present study, it was also found that the relatively mild acid leaching treatment led to some further framework dealumination. This will lower the Brønsted acid site content. However, its effect on performance is surpassed by the positive effect of the removal of EFAl species. It underlines that straightforward parameters as the framework Si/Al obtained from NMR or the unit cell size obtained by XRD are not very useful to predict the real feed hydrocracking performance of USY-based hydrocracking catalysts [50]. Specific to the conversion of heavy feeds is that accessibility of the mesopores and availability of acid sites on the external surface of the zeolite crystals are key to good performance.

We observed that the hydrocracking performance of the acid-leached USY-HT700AL based catalyst was lower than that of the USY-HT700 based one. This is consistent with the observation that acid leaching did not improve the accessibility and acidity of USY-HT700. Moreover, it was seen that additional framework dealumination occurred during acid leaching of USY-HT700. This is also reflected in the highest Lewis-to-Brønsted acidity ratio of all acid-leached samples. It is likely due to the more extensive agglomeration of the EFAl species upon steam treatment at 700 °C, making the acid leaching treatment ineffective. The decreased performance in VGO hydrocracking can therefore be attributed to the significant decrease in Brønsted acidity.

In accord with the literature, it was observed that the middle distillates selectivity decreases with the conversion level [16,51]. When we compare the NiMoP/(USY-HT600AL + Alumina) and NiMoP/(USY-HT500 + Alumina) catalysts, the former afforded more middle distillates at similar conversion. This is probably a consequence of the combination of the lower strong acidity and enhanced mesoporosity, induced by hydrothermal and acid treatment steps that prevent overcracking of the intermediate products [8,12,16]. This observation shows that, by proper choice of steam-calcination and acid-leaching treatment, one can steer the product distribution during VGO hydrocracking using Y zeolites. Of particular importance, the present work shows how mild acid treatments yield to changes in key zeolite properties such as acidity and mesoporosity that are reflected markedly in the hydrocracking performance of a heavy VGO feedstock.

Table 3
Hydrocracking activities of NiMoP-supported catalysts.

Catalyst	Conversion of 370 °C^+ cut, (%)[a]	$Y_{M.D.}/Y_{naphtha}$[b]
NiMoP/(USY-HT500 + Alumina)	32.6	0.78
NiMoP/(USY-HT600 + Alumina)	27.8	0.91
NiMoP/(USY-HT700 + Alumina)	19.3	1.51
NiMoP/(USY-HT500AL + Alumina)	38.5	0.72
NiMoP/(USY-HT600AL + Alumina)	33.4	0.95
NiMoP/(USY-HT700AL + Alumina)	12.4	1.97

[a] Average values after 80 h on stream.
[b] Yield to middle distillates (180–370 °C cut) over yield to naphtha (IPB–180 °C cut).

4. Conclusions

USY zeolites with different degrees of framework dealumination were obtained by changing the temperature of hydrothermal treatment. Corresponding acid leached zeolites were also prepared. The characterization of the zeolites showed that hydrothermal treatment induces progressive framework dealumination, while acid leaching was shown to enhance the textural and acid properties as a result of EFAl extraction. NiMoP based hydrocracking catalysts were prepared using the modified zeolites and evaluated in the hydrocracking of a heavy VGO. Hydrocracking activity of the NiMoP supported catalysts correlates directly with the changes in surface area and acidity of the zeolites. Results indicate that a clear association exists between the degree of dealumination and hydrocracking activity for the catalysts based on steam-treated zeolites. A mild acid leaching treatment to the USY zeolite showed to be beneficial to improve the hydrocracking activity because of the enhanced access to acid sites after the removal of polymerized EFAL species. This study remarks the importance of adjusting the modification conditions to properly tailor the key properties of the USY zeolite as acidity and surface area when used as the main acidic component of a hydrocracking catalyst.

Acknowledgments

The financial support from Instituto Colombiano del Petroleo—ICP, ECOPETROL S.A., for the development of this project is acknowledged. J.L. Agudelo thanks COLCIENCIAS for a Ph.D. scholarship.

Appendix A. Supplementary data

Supplementary data to this article can be found online at http://dx.doi.org/10.1016/j.fuproc.2015.01.011.

References

[1] J.A.R. van Veen, J.K. Minderhoud, L.G. Huve, W.H.J. Stork, Hydrocracking and catalytic dewaxing, Handbook of Heterogeneous Catalysis, Wiley-VCH Verlag GmbH & Co, KGaA, 2008.
[2] G. Valavarasu, M. Bhaskar, K. Balaraman, Mild hydrocracking—a review of the process, catalysts, reactions, kinetics, and advantages, Petroleum Science and Technology 21 (2003) 1185–1205.
[3] J. Scherzer, Hydrocracking Science and Technology, Marcel Dekker, New York, 1995.
[4] C. Martínez, A. Corma, Inorganic molecular sieves: preparation, modification and industrial application in catalytic processes, Coordination Chemistry Reviews 255 (2011) 1558–1580.
[5] M. Rigutto, Cracking and hydrocracking, zeolites and catalysis: synthesis, Reactions and Applications2010. 547–584.
[6] E. Benazzi, L. Leite, N. Marchal-George, H. Toulhoat, P. Raybaud, New insights into parameters controlling the selectivity in hydrocracking reactions, Journal of Catalysis 217 (2003) 376–387.
[7] J.L. Agudelo, B. Mezari, E.J.M. Hensen, S.A. Giraldo, L.J. Hoyos, On the effect of EDTA treatment on the acidic properties of USY zeolite and its performance in vacuum gas oil hydrocracking, Applied Catalysis A: General 488 (2014) 219–230.
[8] K.P. de Jong, J. Zečević, H. Friedrich, P.E. De Jongh, M. Bulut, S. Van Donk, R. Kenmogne, A. Finiels, V. Hulea, F. Fajula, Zeolite Y crystals with trimodal porosity as ideal hydrocracking catalysts, Angewandte Chemie 122 (2010) 10272–10276.
[9] J. Francis, E. Guillon, N. Bats, C. Pichon, A. Corma, L. Simon, Design of improved hydrocracking catalysts by increasing the proximity between acid and metallic sites, Applied Catalysis A: General 409 (2011) 140–147.
[10] Q. Cui, Y. Zhou, Q. Wei, X. Tao, G. Yu, Y. Wang, J. Yang, Role of the zeolite crystallite size on hydrocracking of vacuum gas oil over NiW/Y-ASA catalysts, Energy & Fuels 26 (2012) 4664–4670.
[11] Q. Cui, Y. Zhou, Q. Wei, G. Yu, L. Zhu, Performance of Zr-and P-modified USY-based catalyst in hydrocracking of vacuum gas oil, Fuel Processing Technology 106 (2013) 439–446.
[12] X.-w. Chang, L.-f. He, H.-n. Liang, X.-m. Liu, Z.-f. Yan, Screening of optimum condition for combined modification of ultra-stable Y zeolites using multi-hydroxyl carboxylic acid and phosphate, Catalysis Today 158 (2010) 198–204.
[13] H. Shimada, K. Sato, K. Honna, T. Enomoto, N. Ohshio, Design and development of Ti-modified zeolite-based catalyst for hydrocracking heavy petroleum, Catalysis Today 141 (2009) 43–51.
[14] C. Marcilly, Evolution of refining and petrochemicals: what is the place of zeolites, Oil and Gas Science and Technology 56 (2001) 499–514.
[15] A. Hoek, T. Huizinga, A. Esener, I. Maxwell, W. Stork, F. Van de Meerakker, O. Sy, New catalysts improves heavy feedstock hydro-cracking, Oil and Gas Journal 89 (1991).
[16] P. Dik, O. Klimov, G. Koryakina, K. Leonova, V.Y. Pereyma, S. Budukva, E.Y. Gerasimov, A. Noskov, Composition of stacked bed for VGO hydrocracking with maximum diesel yield, Catalysis Today 220 (2014) 124–132.
[17] H.K. Beyer, Dealumination techniques for zeolites, Molecular Sieves, vol. 3, Springer-Verlag, Berlin, 2002.
[18] C.S. Triantafillidis, A.G. Vlessidis, N.P. Evmiridis, Dealuminated H–Y zeolites: influence of the degree and the type of dealumination method on the structural and acidic characteristics of H–Y zeolites, Industrial and Engineering Chemistry 39 (2000) 307–319.
[19] R. Beyerlein, C. Choi-Feng, J. Hall, B. Huggins, G. Ray, Effect of steaming on the defect structure and acid catalysis of protonated zeolites, Topics in Catalysis 4 (1997) 27–42.
[20] S. Li, A. Zheng, Y. Su, H. Zhang, L. Chen, J. Yang, F.D. Chaohui Ye, Brønsted/Lewis acid synergy in dealuminated HY Zeolite: a combined solid-state NMR and theoretical calculation study, Journal of the American Chemical Society 129 (2007) 11161–11171.
[21] S.M. Almutairi, B. Mezari, G.A. Filonenko, P.C. Magusin, M.S. Rigutto, E.A. Pidko, E.J. Hensen, Influence of extraframework aluminum on the Brønsted acidity and catalytic reactivity of Faujasite zeolite, ChemCatChem 5 (2013) 452–466.
[22] B. Williams, S. Babitz, J. Miller, R. Snurr, H. Kung, The roles of acid strength and pore diffusion in the enhanced cracking activity of steamed Y zeolites, Applied Catalysis A: General 177 (1999) 161–175.
[23] N. Malicki, G. Mali, A.-A. Quoineaud, P. Bourges, L.J. Simon, F. Thibault-Starzyk, C. Fernandez, Aluminium triplets in dealuminated zeolites detected by ^{27}Al NMR correlation spectroscopy, Microporous and Mesoporous Materials 129 (2010) 100–105.
[24] D. Verboekend, G. Vilé, J. Pérez-Ramírez, Hierarchical Y and USY zeolites designed by post-synthetic strategies, Advanced Functional Materials 22 (2012) 916–928.
[25] F.P. Gortsema, R.J. Pellet, A.R. Springer, J.A. Rabo, Catalysts for mid-barrel hydrocracking and process using same, US 5047139 (1991).
[26] A.V. Abramova, E.V. Slivinskii, Y.Y. Goldfarb, A.A. Panin, E.A. Kulikova, G.A. Kliger, Development of efficient zeolite-containing catalysts for petroleum refining and petrochemistry, Kinetics and Catalysis 46 (2005) 758–769.
[27] J. Datka, A. Turek, J. Jehng, I. Wachs, Acidic properties of supported niobium oxide catalysts: an infrared spectroscopy investigation, Journal of Catalysis 135 (1992) 186–199.
[28] S. Van Donk, A.H. Janssen, J.H. Bitter, K.P. de Jong, Generation, characterization, and impact of mesopores in zeolite catalysts, Catalysis Reviews 45 (2003) 297–319.
[29] N.P. Rhodes, R. Rudham, Catalytic studies with dealuminated Y zeolite. Part 1.—catalyst characterisation and the disproportionation of ethylbenzene, Journal of the Chemical Society, Faraday Transactions 89 (1993) 2551–2557.
[30] A. Corma, V. Fornes, F. Rey, Extraction of extra-framework aluminium in ultrastable Y zeolites by $(NH_4)_2SiF_6$ treatments: I, Physicochemical Characterization Applied Catalysis 59 (1990) 267–274.
[31] N. Salman, C.H. Ruscher, J.-C. Buhl, W. Lutz, H. Toufar, M. Stocker, Effect of temperature and time in the hydrothermal treatment of HY zeolite, Microporous and Mesoporous Materials 90 (2006) 339–346.
[32] T. Fleisch, B. Meyers, G. Ray, J. Hall, C. Marshall, Hydrothermal dealumination of faujasites, Journal of Catalysis 99 (1986) 117–125.
[33] M.J. Remy, D. Stanica, G. Poncelet, E.J.P. Feijen, P.J. Grobet, J.A. Martens, a.P.A. Jacobs, Dealuminated H–Y zeolites: relation between physicochemical properties and catalytic activity in heptane and decane isomerization, The Journal of Physical Chemistry 100 (1996) 12440–12447.
[34] Z. Yan, J.Z. Ding Maa, X. Liu, X. Liu, X. Hana, X. Baoa, F. Changb, L. Xub, Z. Liu, On the acid-dealumination of USY zeolite: a solid state NMR investigation, Journal of Molecular Catalysis A: Chemical 194 (2003) 153–167.
[35] A. Omegna, J.A. van Bokhoven, R. Prins, Flexible aluminum coordination in aluminosilicates. Structure of zeolite H-USY and amorphous silica–alumina, The Journal of Physical Chemistry B 107 (2003) 8854–8860.
[36] J. Van Bokhoven, A. Roest, D. Koningsberger, J. Miller, G. Nachtegaal, A. Kentgens, Changes in structural and electronic properties of the zeolite framework induced by extraframework Al and La in H-USY and La (x) NaY: A ^{29}Si and ^{27}Al MAS NMR and ^{27}Al MQ MAS NMR study, The Journal of Physical Chemistry B 104 (2000) 6743–6754.
[37] S.M.C. Menezes, V.L. Camorim, Y.L. Lam, R.A.S.S. Gil, A. Bailly, J.P. Amoureux, Characterization of extra-framework species of steamed and acid washed faujasite by MQMAS NMR and IR measurements, Applied Catalysis A: General 207 (2001) 367–377.
[38] A. Gola, B. Rebours, E. Milazzo, J. Lynch, E. Benazzi, S.L.L. Delevoye, C. Fernandez, Effect of leaching agent in the dealumination of stabilized Y zeolites, Microporous and Mesoporous Materials 40 (2000) 73–83.
[39] I. Halasz, M. Agarwal, B. Marcus, W.E. Cormier, Molecular spectra and polarity sieving of aluminum deficient hydrophobic HY zeolites, Microporous and Mesoporous Materials 84 (2005) 318–331.
[40] N. Malicki, P. Beccat, P. Bourges, C. Fernandez, A.-A. Quoineaud, L.J. Simon, F. Thibault-Starzyk, A new model for acid sites in dealuminated Y zeolites, Studies in Surface Science and Catalysis 170 (2007) 762–770.
[41] S. Khabtou, T. Chevreau, J. Lavalley, Quantitative infrared study of the distinct acidic hydroxyl groups contained in modified Y zeolites, Microporous Materials 3 (1994) 133–148.
[42] P.O. Fritz, J.H. Lunsford, The effect of sodium poisoning on dealuminated Y-type zeolites, Journal of Catalysis 118 (1989) 85–98.
[43] A. Jentys, J. Lercher, Techniques of zeolite characterization, Studies in Surface Science and Catalysis 137 (2001) 345–386.
[44] O. Cairon, Impacts of composition and post-treatment on the brønsted acidity of steam-treated Faujasite: insights from FTIR spectroscopy, ChemPhysChem 14 (2013) 244–251.
[45] A. Corma, A. Martınez, V. Martınez-Soria, Catalytic performance of the new delaminated ITQ-2 zeolite for mild hydrocracking and aromatic hydrogenation processes, Journal of Catalysis 200 (2001) 259–269.
[46] K. Sato, Y. Nishimura, K. Honna, N. Matsubayashi, H. Shimada, Role of HY zeolite mesopores in hydrocracking of heavy oils, Journal of Catalysis 200 (2001) 288–297.
[47] E. Hensen, J. Van Veen, Encapsulation of transition metal sulfides in faujasite zeolite for hydroprocessing applications, Catalysis Today 86 (2003) 87–109.
[48] J. Fierro, J. Conesa, A. Lopez Agudo, Migration of molybdenum into intracrystalline cavities in molybdate-impregnated NaY zeolite, Journal of Catalysis 108 (1987) 334–345.
[49] J. Arribas, A. Corma, V. Fornes, F. Melo, Influence of framework aluminum gradients on the catalytic activity of Y zeolites: cracking of gas–oil on Y zeolites dealuminated by different procedures, Journal of Catalysis 108 (1987) 135–142.
[50] R. Bezman, Relationship between zeolite framework composition and hydrocracking catalyst performance, Catalysis Today 13 (1992) 143–156.
[51] R. Henry, M. Tayakout-Fayolle, P. Afanasiev, C. Lorentz, G. Lapisardi, G. Pirngruber, Vacuum gas oil hydrocracking performance of bifunctional Mo/Y zeolite catalysts in a semi-batch reactor, Catalysis Today 220 (2014) 159–167.